AIAA-95-0298

CONTROL OF EXPERIMENTAL UNCERTAINTIES IN FILTERED RAYLEIGH SCATTERING MEASUREMENTS

J.N. Forkey, N.D. Finkelstein, W.R. Lempert, and R.B. Miles

PRINCETON UNIVERSITY
Dept. of Mechanical & Aerospace Engineering
Princeton, New Jersey 08544 U.S.A.

33rd Aerospace Sciences Meeting and Exhibit
January 9-12, 1995 / Reno, NV

CONTROL OF EXPERIMENTAL UNCERTAINTIES IN FILTERED RAYLEIGH SCATTERING MEASUREMENTS

J. N. Forkey,* N. D. Finkelstein,* W. R. Lempert,† and R. B. Miles‡

Department of Mechanical and Aerospace Engineering
PRINCETON UNIVERSITY
Princeton, New Jersey 08544 U.S.A.
609/258-5131

ABSTRACT

Filtered Rayleigh Scattering is a technique which allows for measurement of velocity, temperature, and pressure in unseeded flows, spatially resolved in 2-dimensions. We present an overview of the major components of a Filtered Rayleigh Scattering system. In particular, we develop and discuss a detailed theoretical model along with associated model parameters and related uncertainties. Based on this model, we then present experimental results for ambient room air and for a Mach 2 free jet, including spatially resolved measurements of velocity, temperature, and pressure.

1. INTRODUCTION

Filtered Rayleigh Scattering (FRS), a recently developed flow diagnostic technique,[1,2] achieves large suppression of background scattering for whole field flow visualization, and obtains quantitative measurements of velocity, temperature and density, in unseeded gaseous flows.

This technique makes use of Rayleigh scattering from molecules in the flow, and is driven by a high power, injection seeded laser. By imaging the scattered light onto a CCD camera, one may obtain an image of flow density. In order to filter out unwanted background scattering from stationary objects in the field of view, the laser is tuned in frequency to coincide with an atomic or molecular absorption line. A cell containing the atomic or molecular species is then placed between the camera and the flow. If the cell temperature, pressure, and length are set appropriately, the absorption line can be made optically thick, so that the cell acts as a notch filter, absorbing all scattering at the laser frequency. Because the flow is moving, the Rayleigh scattering is Doppler shifted, and therefore, passes through the atomic or molecular filter, and is imaged on the camera.

In order to extend the technique to make quantitative measurements, one must take advantage of the fact that the amount of light reaching any resolution element of the camera is a function of the total intensity of the Rayleigh scattering (flow density), as well as the overlap of the Rayleigh scattering profile with the filter absorption profile. This overlap is a function of the central frequency of the Rayleigh profile, which is determined by flow velocity (Doppler shift), and the spectral shape of the Rayleigh profile, which is a function of the flow temperature and pressure. In order to uniquely determine the parameters, v, T, and P experimentally, it is necessary to collect data (resolution element intensity) for varying conditions. A minimum of three data points are required to capture the three parameters. By imaging the scattering through multiple filters with different absorption profiles, or by observing the scattering from several different angles simultaneously, or by monitoring intensity at the camera while tuning the frequency of the laser, it is possible to determine the pertinent parameters of the Rayleigh scattering profile, and, therefore, the velocity, temperature, and pressure at each resolution element.

Previous work has been concentrated into two areas. The first is the use of this technique for background suppression when visualizing flows, and the second is for the measurement of velocity. The background

---

*Graduate Student, Mechanical & Aerospace Engineering, Student Member, AIAA

†Research Scientist, Mechanical & Aerospace Engineering, Member, AIAA

‡Professor, Mechanical & Aerospace Engineering, Senior Member, AIAA

suppression feature of Filtered Rayleigh Scattering has been used to image flow fields that otherwise would be completely obscured by the strong scattering from wind tunnel surfaces. We have used this technique to image the flow field inside a Mach 3 inlet, and to generate volumetric images of the crossing shocks and boundary layers present.[3] Elliot and coworkers[4] have also used this technique to observe structures in compressible mixing layers. Measurements of velocity have been investigated by a number of workers. The measurement of velocity in a seeded compressible mixing layer was performed by Elliot,[5] and velocities over a delta wing in a seeded air flow were measured by Meyers, et. al.[6] using a technique similar to Filtered Rayleigh Scattering, called Doppler Global Velocimetry. The use of Filtered Rayleigh Scattering in unseeded flows for measuring mass flow has been investigated by Winter and Shirley,[7] and velocity measurements in an unseeded Mach 5 flow have been made by our group.

Current work utilizes laser scanning to obtain a complete Rayleigh scattering spectrum for each measurement point. This method of data collection offers the advantage of many data points for model fitting; however, such a method yields time averaged results. The work reported here makes use of two laser/filter pairs. The first consists of a frequency doubled, injection seeded, Nd:YAG laser, along with a molecular iodine absorption cell and the second consists of a frequency tripled, injection seeded, Ti:Sapphire laser along with an atomic mercury filter.

In this paper, we continue the development of Filtered Rayleigh Scattering as a tool for measuring velocity in unseeded flows, by discussing the major sources of systematic uncertainties in FRS experiments, and by discussing techniques that have been developed to minimize these. Although temperature and pressure are measured during an unseeded experiment, these will be discussed only briefly and qualitatively in the results section of this paper; future work will concentrate on quantifying the measurements of these parameters more fully. Our discussion begins with a theoretical model of the scattering and detection processes, which can be used to determine flow parameters from camera intensity values. This is followed by discussions of each of the three major components of a Filtered Rayleigh Scattering experiment -- laser, filter, and camera -- along with corresponding analyses of the major sources of uncertainties, and techniques used to control them. We then demonstrate the utility of FRS by presenting experimental measurements along with a detailed error analysis of the velocity data obtained from an unseeded flow facility and Nd:YAG/iodine filter pair. Two sets of experimental conditions yield velocity fields spatially resolved in two dimensions. We conclude with a discussion of the development of ultraviolet FRS utilizing a frequency tripled Ti:Sapphire laser and a mercury absorption filter. Although the discussions here focus on measurements made using molecular Rayleigh scattering, many of the considerations are directly applicable to experiments which make use of particle scattering.

2. THEORETICAL MODEL

Accurate measurement of flow velocity, temperature and pressure from raw experimental data requires complete understanding of the processes occurring. Furthermore, it is necessary to have an accurate model describing experimental data in order to deduce the measurements of interest. For a Filtered Rayleigh Scattering experiment, the pertinent raw data consists of grayscale value, S, at a particular resolution element of the camera. Our model, therefore, predicts this signal level for any experimental configuration.

When a laser pulse with energy per unit area of E_I, lineshape profile $l(\upsilon)$ and central laser frequency of υ_l, relative to some reference frequency, is incident on a region of flow with pressure P, and temperature T, the Rayleigh scattered energy, E_R at frequency υ relative to the reference frequency, scattered from an interrogation volume V, into the solid angle $d\Omega$, is given by the convolution of the laser lineshape $l(\upsilon)$ and the Rayleigh-Brillouin scattering profile $g(\upsilon)$:

$$E_R(\upsilon) = E_I \frac{PV}{kT}\frac{d\sigma}{d\Omega}d\Omega \int_{-\infty}^{\infty} l(\upsilon - (\upsilon_l + \upsilon_D) - \upsilon')g(\upsilon')d\upsilon' \quad (1)$$

Here, k is equal to Boltzmann's constant, and $\frac{d\sigma}{d\Omega}$ is the differential Rayleigh scattering cross section. The laser lineshape $l(\upsilon)$ is centered at υ_l and shifted by the Doppler shift υ_D:

$$\upsilon_D = \frac{2v}{\lambda}\sin\left(\frac{\theta}{2}\right) \quad (2)$$

where v is the flow velocity in the direction to which the experimental system is sensitive (i.e. v is the velocity component in the direction which bisects the angle between the vector extending from the scattering center to the camera, and the vector pointing opposite the laser propagation vector). λ is the absolute laser wavelength and θ is the scattering angle. The Rayleigh - Brillouin scattering profile, $g(\upsilon)$, is characterized by the Y parameter which is a measure of the ratio of the scattering wavelength to the molecular mean free path.[8,9] This parameter is a measure of the relative contribution of the central Rayleigh scattering peak, and the two side bands corresponding to Brillouin scattering. A Y parameter much greater than one corresponds to strong Brillouin components, while a Y value much less than one corresponds to Rayleigh scattering only. The Y parameter

can be expressed as a function of flow parameters and scattering angle:

$$Y = 0.2308 \left[\frac{T(K)+110.4}{T^2(K)} \right] \left[\frac{P(atm)\lambda(nm)}{\sin\theta/2} \right] \quad (3)$$

In addition to the useful Rayleigh signal, there will also be some stray elastic scattering which has total energy per pulse of K and the same spectral profile and frequency as the laser.

$$E_E(\upsilon) = K\, l(\upsilon - \upsilon_l) \quad (4)$$

When the Rayleigh energy, E_R, and the stray scattering energy, E_E, are passed through the absorption filter, detected by an intensified CCD camera, and converted into a grayscale value by a frame grabber, the final signal level, S (0-255), for one resolution element is given by:

$$S = C\left[\int_{-\infty}^{\infty} E_R(\upsilon) t(\upsilon) d\upsilon + \int_{-\infty}^{\infty} E_E(\upsilon) t(\upsilon) d\upsilon \right] \quad (5)$$

where $t(\upsilon)$ is the transmission of the filter at frequency υ, and C is a constant which takes into account transmission of the focusing optics, quantum efficiency of the camera, gain of the microchannel plate, and analog to digital conversion of the video signal performed by the frame grabber. This equation assumes that the camera gain, and frame grabber A to D conversion are linear and that a value of zero for S corresponds to values of zero for E_R and E_E.

Equations 1 through 5 can be summarized to show explicitly the parameters which influence S:

$$S(\lambda, \theta, R, B, v, P, T, \upsilon_l) = R\frac{P}{T} \times \int_{-\infty}^{\infty} \left\{ \int_{-\infty}^{\infty} l(\upsilon - \left[\upsilon_l + \upsilon_D(v, \lambda, \theta)\right] - \upsilon') g(Y(P, T, \theta), \upsilon') d\upsilon' \right\} t(\upsilon) d\upsilon + B \int_{-\infty}^{\infty} l(\upsilon - \upsilon_l) t(\upsilon) d\upsilon \quad (6)$$

Here, R and B are the products of constants in equations 1, 4 and 5, and in most experiments may be considered calibration parameters. λ is the absolute wavelength of the laser and is necessary only for calculating the Doppler shift and the Y parameter; it is known precisely from the literature. v, P, and T are the unknowns in the experiment. Since these are three independent unknowns, at least three measurements of S must be made while varying $t(\upsilon)$ or at least one of the remaining two parameters : θ, or υ_l. Varying $t(\upsilon)$ corresponds to simultaneous measurements of scattering through different absorption profiles (i.e. different cells). Varying θ corresponds to using either multiple laser angles, or multiple viewing angles and collecting through identical filters. Varying υ_l corresponds to collecting signals at various different laser frequencies. Using multiple θ's, or multiple cells with different $t(\upsilon)$'s, yields instantaneous information about flow parameters. For the work reported in this paper, however, we chose to measure time averaged flow parameters by tuning the laser frequency while monitoring camera signal levels. The main advantage of a time averaged measurement is that high signal levels may be achieved by averaging signal levels from several laser pulses. This minimized the statistical uncertainties caused by shot noise to a negligible level, so that systematic uncertainties could be evaluated and minimized. Additionally, fitting the data to our theoretical model is improved by collecting information at 110 different frequencies.

The raw data obtained in such a frequency tuning experiment consists of plots of resolution element intensity, S, versus laser frequency, υ_l. These plots, one for each image resolution element, are then fit to equation 6 with v, T, and P taken as fitting parameters. In order for such a fit to yield accurate results, all fixed parameters in equation 6 -- λ, θ, R, and B -- must be known, or independently measured. The laser lineshape, $l(\upsilon)$ and the filter cell absorption profile, $t(\upsilon)$, must also be known or independently measured. Any errors in these four parameters or two profiles will propagate into systematic errors in the final values obtained for v, T, and P. Finally, the accuracy of the fit will also depend on the accuracy with which the individual measurements of S and υ_l are made. Any systematic error in S or υ_l will again result in uncertainties in v, T, and P.

3. MODEL PARAMETERS

Each of these four parameters, λ, θ, R, and B, two profiles, $l(\upsilon)$ and $t(\upsilon)$, and two measurement quantities, S and υ_l, along with uncertainties in each is discussed in the following four sections.

Filter

Stability and accurate characterization of the absorption filter are required for the transmission profile $t(\upsilon)$ to be accurately known. The filter used in recent experiments consists of a glass cell 2 inches in diameter and 4 inches long, with 2 inch diameter sleeves extending 2 inches beyond each of the two windows (figure 1). A few iodine crystals were placed in the sealed and evacuated cell. The temperature of the cell is measured and controlled by a temperature controller (stable to within ±0.5 °C), an RTD element cemented onto the cell wall, and heating tape, which covers the entire cell body and sleeves. The pressure of the cell is set by accurately controlling the temperature of a side arm 'cold tip' which

is kept at a lower temperature than the cell body. The side arm is enclosed in a water jacket, and water temperature is controlled by a water bath with a specified temperature accuracy of ±0.01 °C.

In order to characterize the transmission profile of the filter, it is necessary to have a means of accurately measuring the frequency of the interrogation laser relative to some absolute, stable reference. There is also a need to make similar measurements of the laser frequency, υ_l, while performing an actual Filtered Rayleigh Scattering experiment. To this end, we have made use of a heterodyne technique which measures frequency relative to the peak of a Doppler broadened iodine absorption line at 18789 cm^{-1} which corresponds to the P142(37,0) transition in the B-X electronic manifold. The experimental setup used to characterize the absorption filter is shown in figure 2. The laser used as the absolute frequency reference is a Lightwave model 124-1064-50-F narrow linewidth (5 kHz), cw, 50 mW, Nd:YAG laser. A small portion of the infrared light from this laser is frequency doubled using a KTP crystal. The green, frequency doubled light is separated from the infrared light, and passed through a 0.5 inch diameter iodine reference cell of similar construction as the filter cell. The main body of this reference cell is held at a temperature of 80 °C and the sidearm at a temperature of 45.7 °C. The light passed through this reference cell is detected with an amplified photodiode. A standard first derivative nulling technique[10] is used to lock the frequency of the doubled beam of the reference laser to the P142(37,0) absorption peak of the reference cell. The residual infrared laser light from the reference laser is sent through a fiber optic onto a high speed detector (New Focus model # 1434). A second, narrow linewidth, 40 mW, cw, Nd:YAG laser is used to interrogate the original iodine filter cell. This laser beam is also passed through a KTP crystal to generate a frequency doubled beam, which is used to measure transmission through the filter. The residual infrared light from the interrogation laser is passed through the same fiber optic onto the high speed photodetector, where it interferes with the reference laser beam. The interference generates a signal at a frequency equal to the difference between the frequencies of the reference laser and the interrogation laser. A Hewlett Packard microwave frequency counter with accuracy better than 1 MHz measures this heterodyne signal. The frequency difference between the frequency doubled beams is then twice the measured frequency difference between the infrared beams. This system allows for frequency measurements of the frequency doubled beam over a range of 80 GHz.

A computer model of iodine absorption[2] indicates that with a reference cell main body temperature stability of 1°C and side arm temperature stability of 1 °C, the peak of the P142(37,0) transition is stable to within 1 MHz. In order to determine the stability of the frequency of the reference laser, the sensitivity of the feedback electronics must also be considered. To demonstrate the short term stability, the heterodyne beat frequency was monitored while the reference laser was manually detuned, and allowed to re-lock. Because the short term (seconds) stability of the measurement laser is 75 kHz, the change in the beat frequency over this short time period is due solely to the change of the reference laser frequency. As shown in figure 3, the reference laser re-locks to within ± 1MHz of its original frequency. This measurement along with the stability of the reference iodine cell demonstrates the short term frequency stability of this reference signal to be within ±2 MHz. However, in an environment without temperature stabilization, the long term (days) frequency has been observed to shift by as much as a few tens of MHz. This shift is apparent when the system resides in a lab where the temperature cycles through as much as 5 °C in 24 hours. This sensitivity to ambient temperature is probably caused by the particular scheme used to generate the frequency modulation needed for the locking technique. A new frequency modulation scheme with reported sub-MHz stability[10] is currently being assembled. Currently, this long term drift is accounted for by measuring cell transmission versus laser frequency immediately before running a Filtered Rayleigh Scattering experiment, and determining the frequency shift of the reference laser relative to its frequency at the time of the original filter characterization.

Using this frequency measurement technique, the setup in figure 2 was used to determine the transmission profile, $t(\upsilon)$, of the iodine cell. A scan with a resolution of 10 MHz extending over 42 GHz is shown in figure 4. The absorption region used by the current experiments is enlarged in figure 5. The maximum uncertainty on the transmission measurements made with this setup is estimated to be ±0.5%. The maximum uncertainty on the frequency measurements, as discussed above, is estimated to be ±2 MHz. This does not include the long term drift which is accounted for with a calibration experiment at the time of the Filtered Rayleigh Scattering experiment. Three transmission profiles, analogous to figure 4, were taken in a temperature stabilized environment for analysis of FRS data. During data analysis, each of the three spectra were used independently for fitting experimental data to equation 6. The resulting differences in v, T, and P, due to the iodine reference scan that was used were negligible.

Laser

The interrogation laser used in the current experiments is an injection seeded, frequency doubled, pulsed Nd:YAG laser. In order to use equation 6 to analyze experimental data, the absolute wavelength, λ, of the laser, the instantaneous center frequency of the laser, υ_l, relative to the reference laser, and the laser lineshape, $l(\upsilon)$, must all be known, or independently determined.

The wavelength of the laser can be determined from the wavelength of the iodine absorption line used as the

filter. As measured by Gerstenkorn and Luc,[11] this line is located at 18788.4509 cm^{-1} with an uncertainty of ± 0.002cm^{-1}. During the Filtered Rayleigh Scattering experiment, the frequency of the laser is tuned over approximately 5 GHz, which corresponds to a change in wavelength of 0.005 nm. Conservatively, the laser wavelength, λ, which is used to calculate the Doppler shift, equation 2, and the Y parameter, equation 3, may be taken to be 532 nm ± 0.5 nm. This overestimate in the uncertainty of wavelength has negligible effects on the accuracy of measurements of velocity, temperature, and density.

In order to determine the central frequency of the pulsed laser, a small portion of the infrared, cw seed laser is split off from the main beam and combined with the cw infrared beam from the reference laser described above. The same heterodyne system that was used to characterize the filter, is then used to determine the frequency difference between the seed beam and the reference laser. If the central frequency of the pulsed laser is precisely determined by the seed beam, then it is accurately measured by the heterodyne signal. In order to determine how well the pulsed laser frequency matches that of the seed beam, one must know the particular mechanism by which the pulsed laser is locked to the seed laser. For most available lasers, including the laser used in the current experiments, locking is achieved through Q-Switch Buildup Time Reduction (BUTR). This feedback system varies the oscillator cavity length of the pulsed laser while monitoring the time between the firing of the Q-switch and laser emission. When the Q-Switch buildup time is minimized, the pulsed laser is well seeded, and its frequency is very close to that of the seed beam. This feedback system requires that the pulsed oscillator cavity length be continuously dithered, so that even when the pulsed laser is well seeded, its frequency may still oscillate over a small range due to frequency 'pulling' of the output pulse with respect to the seed frequency.[12] This frequency dither is specified by the manufacturer to be less than ±10 MHz at 532 nm. For Filtered Rayleigh Scattering experiments, such as those reported below, that determine flow parameters by fitting data obtained from many laser pulses, the effect of this dither should be negligible, since, on average, half of the laser pulses will have a central frequency up to 10 MHz higher than the measured seed laser frequency, and half will have a central frequency up to 10 MHz lower. For instantaneous measurements, however, this frequency dither must be taken into account if one is to attain accurate velocity measurements.

In addition to this frequency dither, one must also consider the effects of frequency tuning on injection seeding. Scanning of the high power laser is accomplished by stepping the temperature of the seed laser crystal. This changes the crystal length and index of refraction, and therefore, the frequency of the seed laser. By monitoring the frequency of the seed laser after its temperature is changed, it has been determined that the seed laser requires roughly 10 seconds to re-stabilize. Simultaneously, measurements of the feedback voltage to the piezoelectric crystal controlling the cavity length of the pulsed laser show that its frequency has also stabilized after 10 seconds (figure 6). In the experiments reported below, frequency tuning was accomplished by changing the seed laser temperature by discrete steps, and allowing 10 seconds after each step before collecting data. New laser systems currently under development make use of different seeding and tuning techniques, and so the next generation of tunable lasers should be capable of frequency tuning on a shot to shot basis. An alternative locking scheme is further developed in the discussion of future work.

Characterization of the laser frequency profile, $l(\upsilon)$, is also necessary for analysis. A small portion of the pulsed laser beam was passed through the filter cell, and transmission was monitored as a function of laser frequency. The resulting profile is a convolution of the filter profile $t(\upsilon)$, determined as described above, and the laser frequency profile, $l(\upsilon)$. Assuming first a purely Lorentzian laser frequency profile, and then a purely Gaussian profile, a number of data sets were each fit. These fits yielded laser linewidths, for the Lorentzian case, which were much narrower than the frequency transform limit of approximately 150 MHz (based on an infrared laser pulse length of 6 ns). The Gaussian fit, however, yielded more reasonable linewidths between 100 MHz and 200 MHz. An example of this test data and a fit using a Gaussian laser lineshape are shown in figure 7. Although this suggests that the use of a Gaussian lineshape is appropriate, it does not rule out the possibility that some small Lorentzian component is present. In any event, the linewidth of the Rayleigh - Brillouin scattering profile, $g(\upsilon)$, will generally be much broader than the laser linewidth, and so a small discrepancy in the laser lineshape will not introduce a significant error in the flow parameters determined when data is fit to equation 6.

In many laser based diagnostics experiments, it is desirable to continuously monitor the laser intensity, in order to filter out any change in signal due to drift or jitter in laser power. A simple photodiode and boxcar integrator monitoring the intensity of a small portion of the laser beam yielded intensity measurements with uncertainties larger than the small jitter and drift of the laser intensity itself. While a more precise intensity monitoring system may be used in the future, for the experiments reported here, the laser intensity was not continuously monitored, and any small jitter or drift was accounted for in the estimated uncertainties on the parameters R and B as described below.

Camera

The discussion above, outlining the theoretical model, assumes the camera and frame grabber are linear in their response, i.e. that C in equation 5 is independent

of signal level. In order to test the linearity of the imaging system, a cw HeNe laser at 632.8 nm was used to illuminate an index card which was beyond the object plane of the camera. This yielded a temporally stable signal level across the entire CCD chip. With the camera and frame grabber parameters set to the values used in the Filtered Rayleigh Scattering experiments, the camera gate time was reduced in discrete steps, each equal to one tenth the initial value. For an ideal, linear system, this would result in a 10% decrease in signal level at each resolution element with each step. For a very non-linear system response, a calibration experiment such as this could be used to pre-process the signal levels from each resolution element in order to remove non-linearities before the fitting of the data to equation 6. Because the non-linearities appear to be small in this particular camera - frame grabber pair, the current work has not included such pre-processing. However, based on experimental results presented below, this assumption has come to be questioned, especially with regard to threshold values.

The model discussed above, also assumes that the collection solid angle subtended by the camera lens, $d\Omega$, is small enough to consider $\frac{d\sigma}{d\Omega}$, υ_D, $g(\upsilon)$, and $t(\upsilon)$, constants over the entire solid collection angle. In order to determine the conditions for which this assumption is valid, a computer model which does not make this assumption (one which corrects for variation in angle and path length across the imaging lens) was developed, and its results compared to the model above. For this theoretical study, an idealized Mach 5 flow, with velocity equal to 721 m/s, static temperature equal to 50 K, and static pressure equal to 40 torr was assumed. The laser sheet was assumed to have a propagation direction 45° relative to the flow, and the camera was assumed to image at a nominal angle of 90° to the sheet. Filter transmission versus frequency plots were calculated for the point in the center of the field of view, using this more detailed model, assuming various collection f numbers (distance from lens to laser sheet / diameter of lens). These plots were compared to similar plots made using the simpler theory discussed above. As can be seen in figure 8, a very small collection f# results in very different curves for the two models. This is to be expected, since the scattering angle θ, varies significantly across the solid collection angle $d\Omega$, resulting in large variations in Doppler shift υ_D, and scattering profile $g(\upsilon)$. As the collection f# increases, the variation of θ across the solid collection angle decreases, and so the discrepancy between the two models also decreases. For a collection f# greater than about 10, this discrepancy is small enough to be considered negligible.

For the experiments discussed below, the collection f# was approximately 15, so the variation in θ across the solid collection angle was neglected. It was still necessary, however, to determine the value of θ accurately in order to obtain v, T, and P with low uncertainties. The difficulty with the measurement of this angle is that there exists no convenient marker for the camera observation direction. In order to address this problem, a HeNe laser at 632.8 nm was positioned so that the beam was coincident with the central camera observation ray. The center of the camera lens, and the center of the field of view uniquely define this ray. By placing an index card in the HeNe beam at various locations, a spot was observed on the CCD chip. When the index card was in the object plane of the camera lens, the laser spot appeared as a small, focused spot; when the card was behind or in front of the object plane, the spot appeared as a much larger unfocused spot. The position and angle of the HeNe laser beam were varied until the in focus spot and out of focus spot were both centered on the central pixel of the CCD chip. At this point the HeNe laser precisely overlapped the main camera ray, and was, therefore, an accurate indicator of the observation direction. The scattering angle, θ, was then measured by observing, on a protractor, the angle between the incident Nd:YAG laser beam and the HeNe beam. The accuracy of this technique was limited by the accuracy with which the protractor could be read, and was estimated to be $\pm 1°$. In larger facilities this same technique could be used to obtain much more accurate angle measurements since a triangulation scheme could be used, where the lengths of three sides of a triangle composed of the Nd: YAG beam, the HeNe beam, and a line between them could be measured with small relative uncertainty.

Other Parameters

In the discussion of the theoretical model presented above, it was shown that uncertainties in the fitted flow parameters v, T, and P are dependent on the uncertainties in four fixed model parameters, λ, θ, R, and B, two profiles, $l(\upsilon)$ and $t(\upsilon)$, and two measurement quantities, S and υ_l. The previous three sections have discussed all of these uncertainties with the exception of the two model parameters R and B. Both of these parameters depend critically on the particular experimental setup, and, therefore, cannot be predicted with even marginal accuracy from theoretical considerations. Although they could be taken as two additional fitting parameters, this would decrease the certainty with which v, T, and P could be determined from the fit. Therefore, pre and post experiment calibrations were used to measure these two values to within some range. Two calibrations were performed, both with the filter cell removed from the front of the camera, thereby allowing for a $t(\upsilon)$ profile of 1 (i. e. the absence of the filter cell is equivalent to the presence of a filter cell with 100% transmission at all frequencies). In the first calibration, the camera imaged an evacuated test section. With P equal to zero, and $t(\upsilon)$ equal to 1, equation 6 becomes: S=B. For the second calibration, the camera imaged the test section at atmospheric conditions. In this case, P was assumed to be equal to 760 torr, and T was approximately 293 K (T was

measured with a thermocouple for each calibration run). Equation 6 now becomes $S = \frac{P}{T}R + B$, and since B is known from the first calibration, R can be determined. Typical values and uncertainties for R and B are 600± 20 and 40 ± 5, respectively.

4. MEASUREMENTS

Experimental Set-Up and Data Collection

In order to demonstrate the measurement capability of the Filtered Rayleigh Scattering technique, we have performed experiments under two test conditions. The first condition consists of ambient air at room temperature and pressure (nominally 20°C and 760 torr). Although the air is not moving, this test is still a good indicator of the accuracy of the velocity measuring capabilities of Filtered Rayleigh Scattering for the given temperature and pressure conditions, since the major uncertainties on the velocity measurement are expected to be absolute, not relative. The second test condition consists of a Mach 2 free jet pressure matched to ambient atmospheric pressure.

The experimental setup for these experiments is shown in figure 9. The frequency doubled, injection seeded, pulsed laser described above was used as the laser source. The beam was focused into a sheet and passed through the 6 inch by 6 inch vertical test section of a laboratory scale wind tunnel, at an angle of roughly 50 degrees to the vertical. The intensified CCD camera and zoom lens, captured scattered light at 90 degrees to the laser sheet. The iodine cell discussed above was placed between the camera lens and the flow to be used as the absorption filter. The first test condition of ambient room air was achieved by temporarily removing the windows on the test section before the experiment was performed, and by leaving opened a valve between the test section and the surrounding laboratory during the experiment. For the second test case, compressed atmospheric air was passed through a nozzle contoured to produce a Mach 2 flow which is pressure matched to atmospheric pressure. The stagnation pressure was held at 100psig, and the stagnation temperature was measured to be 258 K. Isentropic calculations predict that the free stream velocity, static temperature, and static pressure at the exit of this jet should be 480 m/s, 143 K, and 753 torr. In order to achieve a significant Doppler shift, the Nd:YAG beam crossed the flow at an angle of 50°. This required that the measurement region in the flow be some 12 mm to 22 mm (or 2 to 4 nozzle diameters) downstream of the nozzle exit in order to keep the laser beam from hitting the nozzle. RELIEF experiments[13] performed along a line 19 mm from the nozzle exit yielded velocities varying from 477 m/s to 497 m/s. This variation indicates the flow in the FRS test region has already interacted with the shear layers, and so velocity, temperature, and pressure values are not expected to be uniform, nor identical to the isentropically calculated values.

For each of the two test conditions, the experimental procedure consisted of first running calibrations, then taking experimental data, and concluding with calibration runs. Measurements of resolution element intensity, S, were taken when the test section was evacuated, and again when filled with air at atmospheric pressure and temperature. These data determined values for R and B, as discussed above. Additionally, during the calibration runs, a portion of the laser beam passed directly through the iodine absorption cell in order to determine a transmission versus frequency profile. This profile was then used to determine any long term frequency offset of the reference laser frequency, which may have occurred since the filter cell was characterized. The same profile was used to determine the laser linewidth as discussed above. Next, the filter was placed in front of the camera, and the flow was imaged at 110 different laser frequencies. Fifty frame averages were stored at each frequency. Finally, calibrations were again performed in order to detect any drifts in R, B, frequency offset, or laser linewidth during the run. The average of two values determined for each of R, B, frequency offset, and laser linewidth were subsequently used when analyzing the data.

Data analysis consisted of binning the camera pixels into 10 pixel by 10 pixel resolution elements, which correspond to roughly 300 micron by 300 micron points in the flow. The size of these resolution elements was determined by previous work which indicated that the resolution of the microchannel plate was effectively 5 pixels by 5 pixels on the CCD chip.[14] At each resolution element, an intensity versus frequency curve was generated, and then fit to equation 6 using parameter values, λ, θ, R, and B, and lineshape profiles, $t(\upsilon)$ and $l(\upsilon)$, all of which were determined either during the calibration scans, or measured before the experiment as described in the sections above. Such data, S versus υ_l, and the associated final fit to the model for a particular resolution element of the ambient air test conditions is shown in figure 10. These fits, one at each resolution element, yielded values for v, T, and P at each point in the flow.

Uncertainty Analysis

In order to estimate the uncertainties associated with the final measurements of velocity, the uncertainties in the parameters λ, θ, R, and B, and the uncertainties in the lineshape profiles $t(\upsilon)$ and $l(\upsilon)$ were all taken into account for one test point in the field of view for each of the two test measurement configurations. It is possible to independently calculate uncertainty measurements for velocity, temperature, and pressure at every point in the field of view. However, here, we present only a sample analysis of velocity uncertainty estimates at a point in the center of the field of view for the two conditions, ambient

air and a Mach 2 jet. Each of the individual uncertainties in the four parameters λ, θ, R, and B propagates into uncertainties in velocity, in the following manner, analogous to:[15]

$$\Delta v = \frac{\partial v}{\partial \theta}\Delta\theta \qquad (7)$$

Here, the uncertainty in velocity, Δv, due to an uncertainty in angle, $\Delta\theta$, is given. The uncertainty in λ is determined as discussed above. The uncertainty in θ was estimated when it was measured. The uncertainties in R and B are estimated based on the variations between the pre and post calibration measurements at the various points in the test region.

In order to take into account the uncertainty of velocity due to uncertainty in the lineshape $l(\upsilon)$, the following equation is used:

$$\Delta v = \frac{\partial v}{\partial(\delta\upsilon)}\Delta(\delta v) \qquad (8)$$

where $\delta\upsilon$ is equal to the linewidth of the laser profile $l(\upsilon)$ of the assumed Gaussian lineshape, which is obtained from the fits to the pre and post calibration experiments. Finally, systematic uncertainties in υ_l arising due to uncertainty in the amount of the long term drift of the reference frequency were accounted for with equations of the form:

$$\Delta v = \frac{\partial v}{\partial \upsilon_r}\Delta\upsilon_r \qquad (9)$$

where here, υ_r, is the reference frequency. The uncertainty in linewidth, $\delta\upsilon$, and the long term drift of the reference frequency υ_r, are estimated based on pre and post calibration values for a number of experiments. All of the partial derivatives in equations 6 through 8, except $\frac{\partial v}{\partial \theta}$, are calculated numerically by fitting the data with the appropriate parameter changed slightly. $\frac{\partial v}{\partial \theta}$ is calculated analytically, by using equation 2. In order to combine all of the individual contributions to the uncertainty in velocity, we assumed the individual uncertainties were uncorrelated, and took the square root of the sum of the squares[15] as the total systematic uncertainty. Table 1 summarizes the uncertainties in each of the parameters and profiles, shows the relevant partial derivatives at the test point for the first set of test conditions, and the uncertainty in velocity attributed to the uncertainty in each of the parameters and profiles. The final estimated uncertainty in velocity is 4 m/s. Table 2 shows the same data for the second test case (Mach 2 free jet). The final estimated uncertainty for this case is 5 m/s.

par	λ (nm)	θ (deg)	R	B	$\delta\upsilon$ (MHz)	υ_r (MHz)	Total Uncert ainty
typ. value	532.	91	600	40	150	--	
Δpar	0.5	1	20	5	50	5	
$\frac{\partial v}{\partial(\text{par})}$	0.013	0.011	0.008	0.25	0.002	0.65	
Δv (m/s)	0.007	0.011	0.16	1.25	0.1	3.25	3.5

Table 1: Uncertainties for velocity measurement in ambient air

par	λ (nm)	θ (deg)	R	B	$\delta\upsilon$ (MHz)	υ_r (MHz)	Total Uncert ainty
typ. value	532.	91	600	40	150	--	
Δpar	0.5	1	20	5	50	5	
$\frac{\partial v}{\partial(\text{par})}$	0.38	0.41	0.004	0.91	0.002	0.44	
Δv (m/s)	0.19	0.41	0.08	4.55	0.1	2.2	5.1

Table 2: Uncertainties for velocity measurement in Mach 2 jet.

These tables demonstrate, in both cases, that velocity is most sensitive to variations in B, the background scattering level, and υ_r, stability of the frequency reference. Now that these parameter uncertainties have been reduced to acceptable levels, experiments can focus on identifying error sources that had been previously masked.

Experimental Results

Results from the first test case are shown in color figure 1. This plot shows velocity, in the direction of sensitivity, as a function of downstream and spanwise location. The background here has been artificially set to a very low velocity delineated by dark red. The actual data is shown throughout the laser sheet which extends from the top right of the plot to the bottom left. Measured velocity values within the sheet range from -12 m/s to 31 m/s. The errors in these velocity measurements are considerably larger than the predicted uncertainty in Table 1. Because the uncertainties associated with the parameters listed in Table 1 are small, the larger errors must be due to other factors. A comparison of color figure 1 with color figure 2, which shows the calibration parameter R, indicates that the variations in measured velocity are correlated with variations in the magnitude

of R. However, the variation in R is caused primarily by the spatial profile of the laser. This correlation suggests the measured velocity depends on the recorded laser intensity. This is probably an artifact of the non-linearity of the detection system, which was neglected in the original analysis. The observed correlation between measured velocity value and laser intensity suggests that even a small amount of non-linearity in the detection system causes uncertainties in the velocity measurement. Once this non-linearity is accounted for, a variation in measured values closer to the predicted value of ±4 m/s can be expected. In particular, the region at the top of the laser sheet, with low laser energy (less than 75% of the peak), accounts for most of the distribution in measured velocity. Neglecting this small portion of the laser sheet yields a measured velocity range between -12 m/s and 10 m/s.

Velocity values obtained with the Mach 2 free jet are shown in color figures 3 and 4. In these figures, the values in the region outside of the laser beam have been artificially set to 0 m/s (yellow). The core of the jet can clearly be seen as the violet region, while the shear layers are apparent on either side of the core, extending from the violet region near 200 m/s to the yellow zero values. It should be emphasized that the measured velocity is the velocity component along the direction of sensitivity, which is determined by the laser propagation direction, and the camera observation direction. Points outside of the flow, but still within the laser sheet were analyzed and assigned their measured velocity values, all of which were close to 0 m/s, as evidenced by the fact that the laser sheet cannot be differentiated from the background, outside the jet. The velocity measurements within the core of the jet vary from 192 m/s to 221 m/s. Again, some of this distribution in velocity is generated by the variation in laser intensity across the laser sheet. However, much of it is probably due to a real variation in velocity at this point in the flow. Evidence of such variations have been observed previously during RELIEF experiments performed with a tag line at 19mm from the nozzle exit. These RELIEF experiments yielded values for free stream velocity. After correcting for a slight difference between stagnation temperature, the RELIEF experiments predict free stream velocities ranging from 477 m/s to 497 m/s.

In order to project from the velocity in the direction of sensitivity of the Filtered Rayleigh Scattering experiment, to the velocity in the free stream direction, the angle between the direction of sensitivity and the free stream must be measured. For an angle of 65.5°, the Filtered Rayleigh Scattering velocities would be in precise agreement with the RELIEF velocities. During the FRS experiment, this angle was measured by assuming that the free stream direction was perpendicular to the flat top of the nozzle exit. All angles were measured, therefore, with the flat nozzle top being taken as a reference. Using this technique, the angle between the direction of FRS sensitivity and the free stream was determined to be 62.7° ± 0.7°. The 2.0° to 3.4° discrepancy between this angle and the required 65.5°, is probably due to a slight deviation between the free stream direction and the direction perpendicular to the flat top of the nozzle exit. It should be emphasized that the difficulty in measuring the angle between the direction of velocity sensitivity and the free stream velocity is not unique to Filtered Rayleigh Scattering. This issue will be important in any technique that measures Doppler shift to determine one component of velocity.

Although the temperature and pressure data obtained from the Filtered Rayleigh Scattering experiments has not yet been fully analyzed, we present here preliminary plots of this data for the Mach 2 conditions. Color figures 5 and 6 show 3-D plots of temperature and pressure. Both show behavior of the parameters as expected. The pressure of the free jet appears to be the same as that of the ambient surroundings, as expected, although the pressure values vary significantly across the entire region of interest. The temperature of the free jet is seen in color figure 6 to be significantly lower than that of the ambient, also as expected. Although the variation of measured temperature across the jet is ± 17 K, the average value of 142 K matches the isentropically calculated value well.

5. FUTURE WORK

This work has emphasized control of experimental uncertainties to minimize the systematic uncertainties associated with Filtered Rayleigh Scattering. However, statistical uncertainties must also be considered. Signal to noise limitations arise primarily due to shot noise. In order to reduce this statistical uncertainty to below 1%, it is necessary to collect 10,000 photo-electrons per resolution element. Earlier discussions[16] for realistic conditions, using the Nd:YAG/iodine FRS paradigm, and f5 optics, conclude that a CCD camera generates 64 photo-electrons per resolution element per laser pulse. This yields measured intensity variation of 1 part in 8, or 12.5%. Time averaging, however, allows for the collection of a larger number of photons. By averaging 160 laser pulses, or 16 seconds at 10 Hz repetition rate, at each measurement point, the shot noise is reduced below 1%. However, this scheme prevents instantaneous measurements. Because the Rayleigh scattering cross-section increases dramatically in the ultraviolet, due to the frequency, υ^4, and index of refraction, $(n-1)^2$, scaling, it is possible to collect in excess of 600 photo-electrons per laser pulse at 253.7 nm for the same experimental setup. The single pulse shot noise is reduced to an uncertainty of 2.4%.

Applying the Titanium:Sapphire/Hg Filter paradigm to FRS, yields noticeable improvements both because of the laser and filter characteristics. Current efforts to complete a high power, narrow linewidth, tunable ultraviolet laser system are underway. By injection seeding a pulsed Ti: Sapphire, and frequency tripling the tunable infrared output, we achieve in excess of 10 mJ of

tunable, narrow linewidth, ultraviolet light. To insure single mode operation while the laser is frequency tuned, efforts to complete injection locking of the pulsed Ti: Sapphire are underway. To avoid the necessarily slow tuning rate of the BUTR injection locking technique of the Nd:YAG, a novel method of injection locking via a fringe locking technique is being developed in collaboration with Schwartz Electro-Optics, Inc.[17] The implication of such a locking technique is that the feedback is given on an instantaneous basis, rather than on the shot to shot basis of the BUTR. Feedback to the locking system is given between laser pulses, and thus, tracking by this system offers a frequency agile laser. Tuning may be faster, take discontinuous jumps, or dither over a wide range, without fear of unlocking.

The development of a novel atomic vapor filter for FRS, using mercury, allows for a variety of improvements, as well. Because of the strong absorption and high atomic weight of mercury, achieving very high optical depth is attainable. Model fits to experimental transmission scans of a 5 cm length mercury vapor filter, suggest optical depths in excess of 1000.[17] A detailed scan of the Hg 202 line for a sidearm temperature of 23 C (figure 11), demonstrates the nearly ideal characteristics of a mercury vapor filter. The high optical depth translates into an ability to suppress very strong elastic scattering, while transmitting weaker Doppler shifted signals, as would be desirable for imaging air flow over a model (or imaging a boundary layer). Mercury does not suffer the background absorption difficulties of iodine. As a result, it is possible to dramatically vary the width of the absorption profile of the filter. This leads to the tailoring of filters to an appropriate experiment and to the use of multiple filters for instantaneous measurement of T, P, v. As previously mentioned, iodine experiments to date relied on scanning laser frequency; however, multiple Hg filters may be used with varying transmission profiles, to extract the same information on an instantaneous basis. Alternately, it may be possible to affect the mercury cell linewidth with an applied magnetic field. Then, a single cell could be rapidly 'scanned' to achieve multiple measurements for instant calibration, and achieve several data points for varying absorption profiles, $t(\upsilon)$.

6. SUMMARY

The major components of a Filtered Rayleigh Scattering experiment have been examined and sources of systematic uncertainty have been identified and controlled to acceptable levels. With these sources of uncertainty reduced, current experimental results may now be used to determine other sources of uncertainty which had previously been masked. Work continues on the development of an UltraViolet Filtered Rayleigh Scattering system which will allow for reduction of statistical uncertainty.

ACKNOWLEDGMENTS

We would like to thank Professor Tenti, University of Waterloo, for making available to us his program for calculating Rayleigh Brillouin profiles.

This work was conducted under the support of the Air Force Office of Scientific Research, NASA-Langley, NASA-Lewis, and Small Business Innovative Research Programs under M.L. Energia, Inc. and Schwartz Electro-Optics, Inc.

REFERENCES

1. R.B. Miles and W.R. Lempert, "Two Dimensional Measurement of Density, Velocity, and Temperature, in Turbulent High Speed Air Flows by UV Rayleigh Scattering," Applied Physics B, Vol. 51, pg. 1, 1990.

2. R.B. Miles, J.N. Forkey, and W.R. Lempert, "Filtered Rayleigh Scattering Measurements in Supersonic/ Hypersonic Facilities," 7th Aerospace Ground Testing Conference, Nashville, TN, July 1992. AIAA-92-3894

3. J.N. Forkey, W.R. Lempert, S.M. Bogdonoff, G.Russell, and R.B. Miles, "Volumetric Imaging of Supersonic Boundary Layers Using Filtered Rayleigh Scattering Background Suppression," 32nd AeroSciences Meeting and Exhibit. Reno, NV, Jan. 1994. AIAA 94-0491.

4. G.S. Elliot, M. Samimy, and S.A. Arnett, "A Study of Compressible Mixing Layers Using Filtered Rayleigh Scattering, " 30th AeroSciences Meeting and Exhibit. Reno, NV, Jan. 1992. AIAA 92-0175.

5. G.S. Elliot, M. Samimy, and S.A. Arnett, "Details of A Molecular Filter Based Velocimitry Technique," 32nd AeroSciences Meeting and Exhibit. Reno, NV, Jan 1994. AIAA 94-0490.

6. J.F. Meyers, "Development of Doppler Global Velocimetry," 18th Aerospace Ground Testing Conference, Colorado Springs, CO, June 1994. AIAA 94-2582.

7 M. Winter and J.A. Shirley, "Air Mass Flux Measurement System Using Doppler Shifted Filtered Rayleigh Scattering, " 31st AeroSciences Meeting and Exhibit. Reno, NV, Jan. 1993. AIAA 93-0513.

8. G. Tenti, C.D. Boley, and R.C. Desai, "On the Kinetic Model Description of Rayleigh-Brillouin Scattering From Molecular Gasses, " Canadian Journal of Physics, Vol. 52, pg. 285, Feb. 1974.

9. H. Shimizu, S.A. Lee, and C.Y. She, "High Spectral Resolution Lidar System with Atomic Blocking Filters for Measuring Atmospheric Parameters, " Applied Optics, Vol. 22, pg. 1373, 1983.

10. A. Arie, M.L. Bortz, M.M. Fejer, and R.L. Beyer, "Iodine Spectroscopy and Absolute Frequency Stabilization with the Second Harmonic of the 1319-nm Nd:YAG laser," Optics Letters, Vol. 18, pg. 1757, 1993.

11. S. Gerstenkorn, and P. Luc, Atlas du Spectre d'Absorption de la Molecule Diode, Part 3, pg. 53, 1978.

12. Y.K. Park, G. Guiliani, and R.L. Beyer, "Unstable Single-Axial-Mode Operation of an Unstable Resonator Nd:YAG Oscillator by Injection Locking, " Optics Letters, Vol. 5, pg. 96, 1980.

13. R.B. Miles, J. Connors, E. Markovitz, P. Howard, and G. Roth, "Instantaneous Supersonic Velocity Profiles in an Under Expanded Sonic Air Jet by Oxygen Flow Tagging, " Physics of Fluids A, Vol. 1, pg. 389, 1989.

14. personal communication: Kyritsis, D., Engine Lab., Mechanical and Aerospace Engineering Department, Princeton University, Princeton, NJ.

15. see, for example, P.R. Bevington Data Reduction and Error Analysis for th e Physical Science, Mc Graw Hill, 1969.

15. R.B. Miles, J.N. Forkey, N.D. Finkelstein, and W.R. Lempert, "Precision Whole-Field Velocity Measurements with Frequency Scanned Filtered Rayleigh Scattering," 7th International Symposium on Application of Laser Techniques to Fluid Mechanics, Lisbon, Portugal, July 1994.

16. N.D. Finkelstein, J.Gambogi, W.R. Lempert, R.B. Miles, G.A. Rines, A. Finch, and R.A. Schwarz, "Development of a Tunable Single Frequency UltraViolet Laser Source for UV Filtered Rayleigh Scattering" 32nd AeroSciences Meeting and Exhibit. Reno, NV, Jan. 1994. AIAA 94-0492.

FIGURES

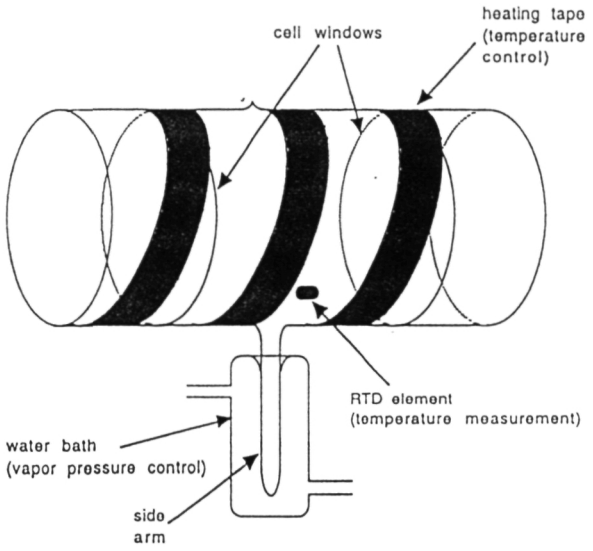

Fig. 1: Iodine absorption cell.

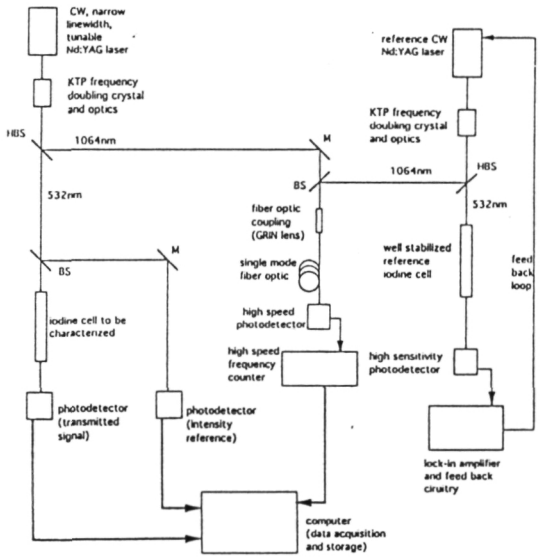

Fig. 2: Experimental setup used to characterize iodine cell. Frequency reference is on the right, and the transmission measurement setup is on the left. Abbreviations are: BS - beamsplitter, HBS - harmonic beam splitter, M - mirror

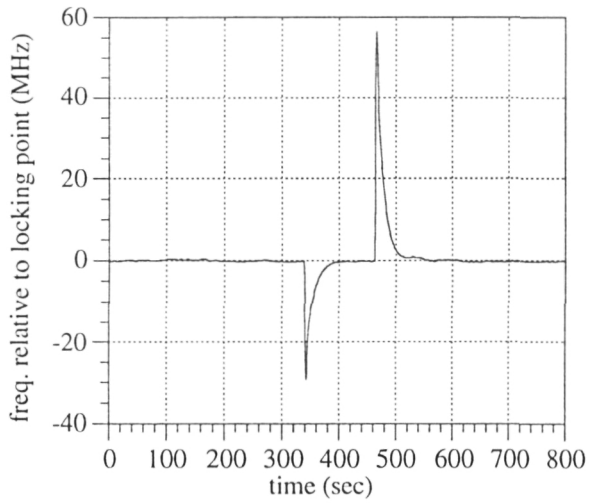

Fig. 3a: Demonstration of re-locking of reference laser after manual de-tuning.

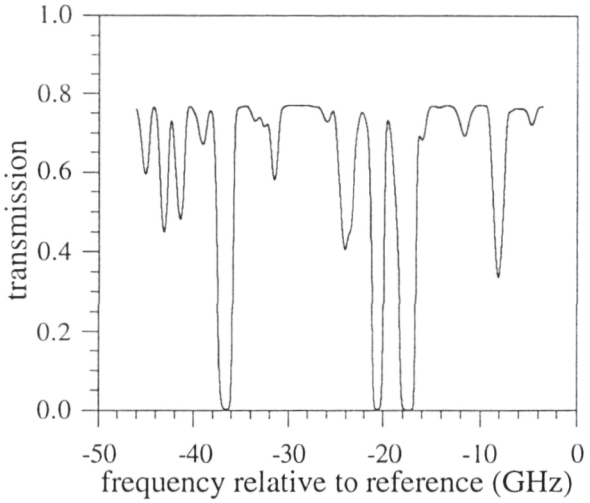

Fig. 4: Transmission profile of iodine filter cell

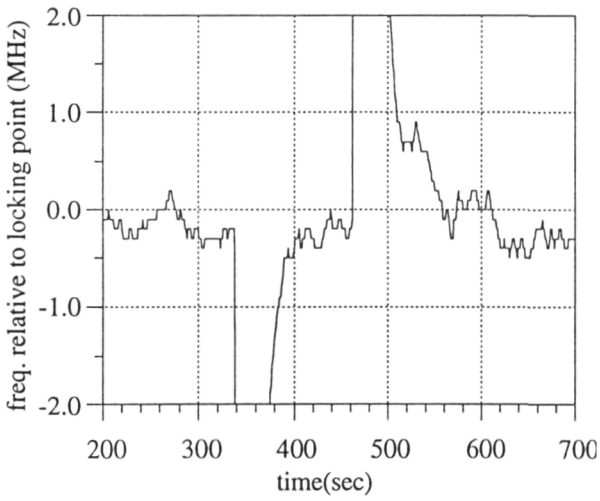

Fig. 3b: Enlargement of figure 3a, showing the reference laser re-locking to within ±1 MHz.

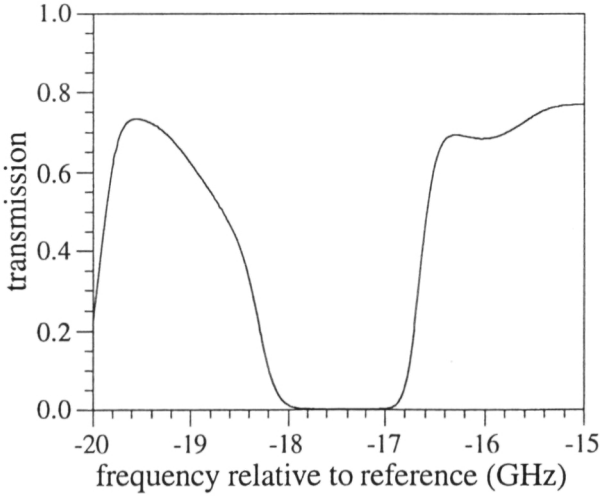

Fig. 5: Detail of filter transmission profile

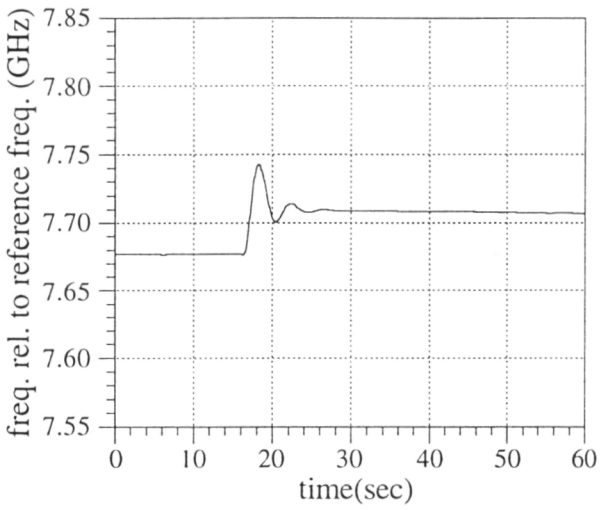

Fig. 6a: Frequency of injection seeder after a discrete change in tuning voltage

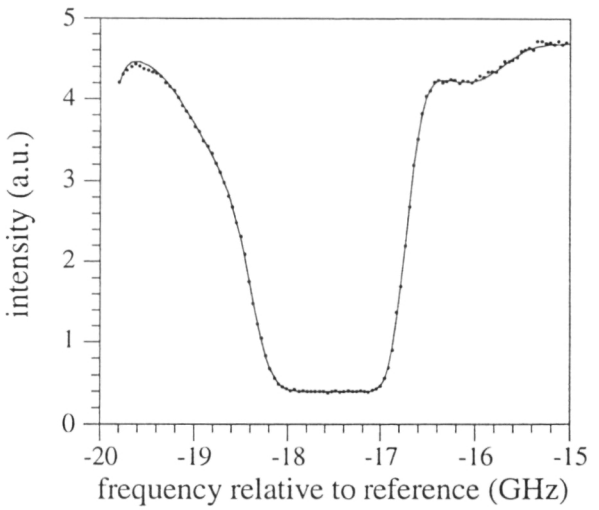

Fig. 7: Fit of calibration data (points) to a convolution between the Gaussian laser line profile and the filter transmission profile (line)

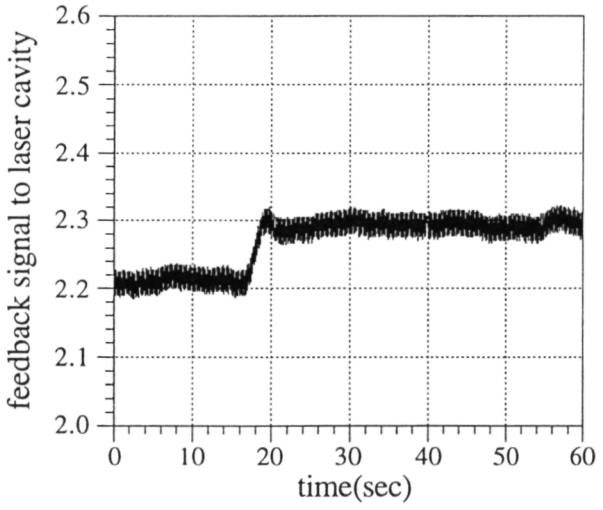

Fig. 6b: Feedback signal which controls locking of laser by changing oscillator cavity length

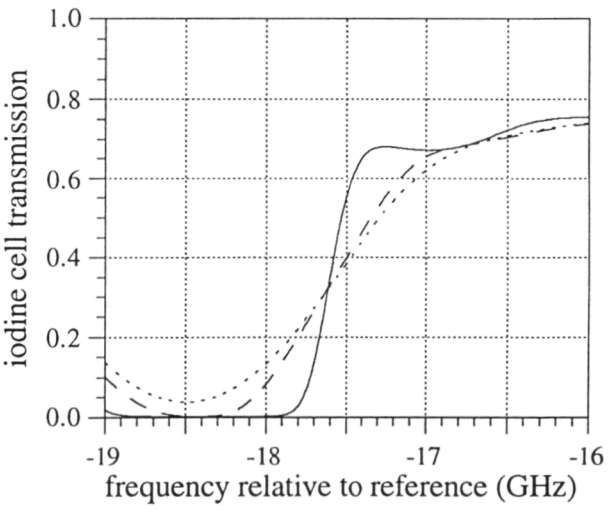

Fig. 8a: Response of the iodine filter to scattering from an idealized Mach 5 flow, imaged with a collection f# of 1. The solid curve shows the response predicted for narrow linewidth scattering when effects of the solid collection angle are neglected. The dashed line includes the effects of the solid collection angle, again assuming narrow linewidth scattering. The dotted line includes the effects of the solid collection angle, as well as the Rayleigh-Brillouin scattering profile.

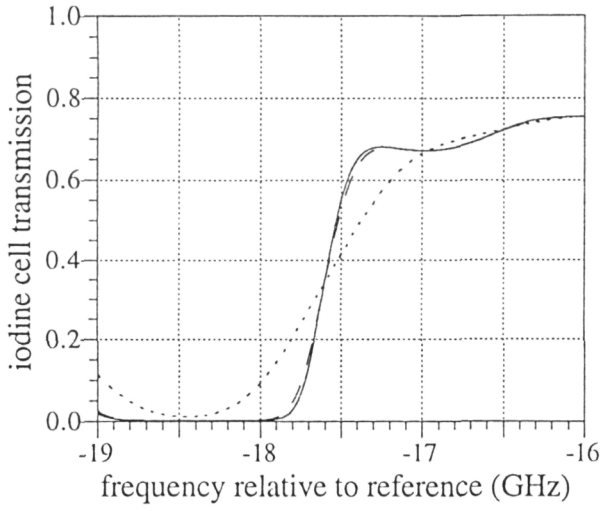

Fig. 8b: Response of the iodine filter to scattering from an idealized Mach 5 flow, imaged with collection f# of 5

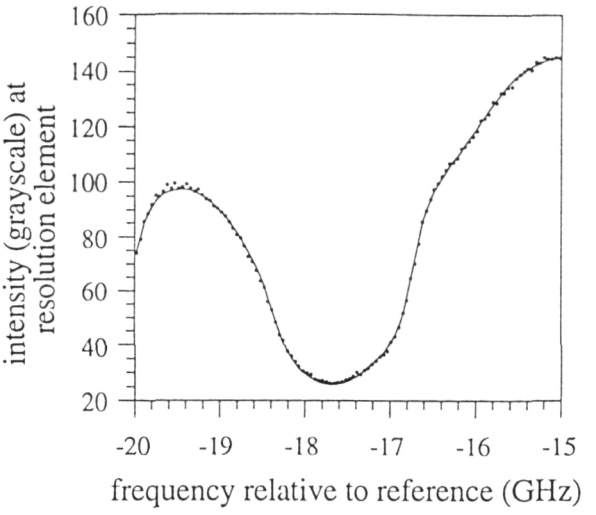

Fig. 10: Fit of grayscale data values at one resolution element (points) to S(υ) as given by equation 6 (line).

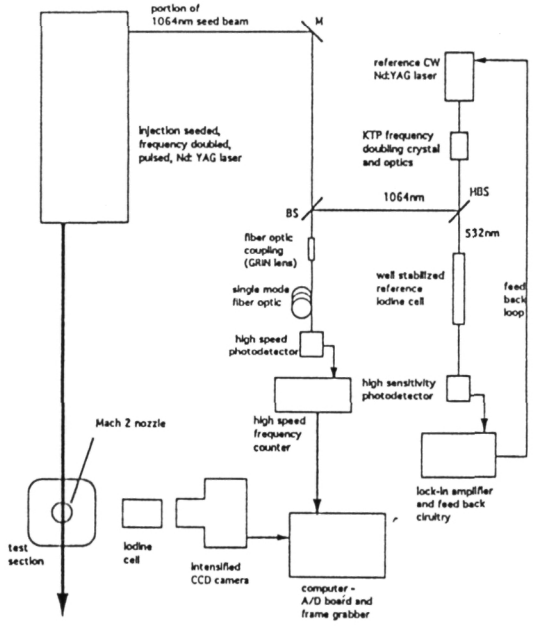

Fig. 9: Experimental setup for Filtered Rayleigh Scattering experiments. Abbreviations are as in fig. 2.

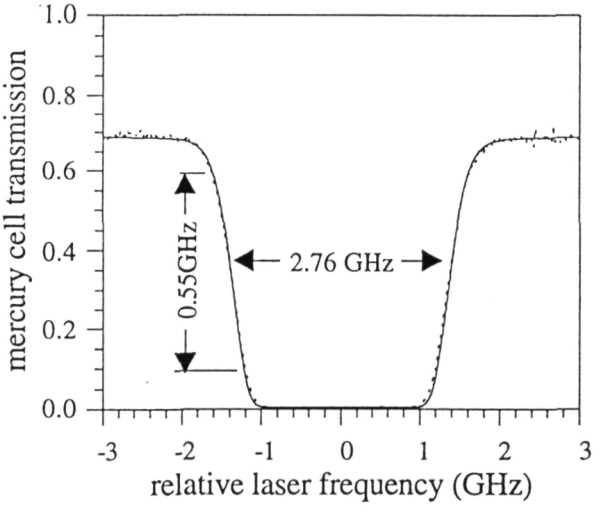

Fig. 11: Experimental scan of mercury vapor cell transmission (dotted) at 253.7 nm for a 5 cm long cell with a cell temperature of 48°C, and a side arm temperature of 23°C. Fit to theory (solid) yields an optical depth of 71.